analytical chemistry

pubs.acs.org/ac

Article

FT-ICR MS Spectral Improvement of Dissolved Organic Matter by the Absorption Mode: A Comparison of the Electrospray Ionization in Positive-Ion and Negative-Ion Modes

Qing-Long Fu,* Chao Chen, Yang Liu, Manabu Fujii, and Pingqing Fu

Cite This: *Anal. Chem.* 2024, 96, 522−530

Read Online

ACCESS | Metrics & More | Article Recommendations | Supporting Information

ABSTRACT: Fourier transform ion cyclotron resonance mass spectrometry (FT-ICR MS) in the absorption mode has a superior performance over the conventional magnitude mode. However, this improved performance for the analysis of dissolved organic matter (DOM) in negative-ion and positive-ion modes of electrospray ionization [ESI(−) and ESI(+), respectively] remains unknown. This study systemically compared the improved performance by the absorption mode for DOM FT-ICR MS spectra acquired with the low-field and high-field magnet instruments between two charge modes. The absorption mode enhanced the resolution and signal-to-noise ratio values of DOM peaks with factors of 1.88−1.94 and 1.60−1.72, respectively. The significantly higher improvement of mass resolution for the ESI(+) mode than that for the ESI(−) mode could resolve the extensive occurrence of mass doublets in the ESI(+) mode, yielding some formulas exclusively identified in the ESI(+) mode. The findings of this study have systemically demonstrated the superiority of the absorption mode in improving the spectra quality during the routine FT-ICR MS postdata analysis and highlighted its great potential in characterizing the molecular composition of DOM using the FT-ICR MS technique in both ESI(−) and ESI(+) modes.

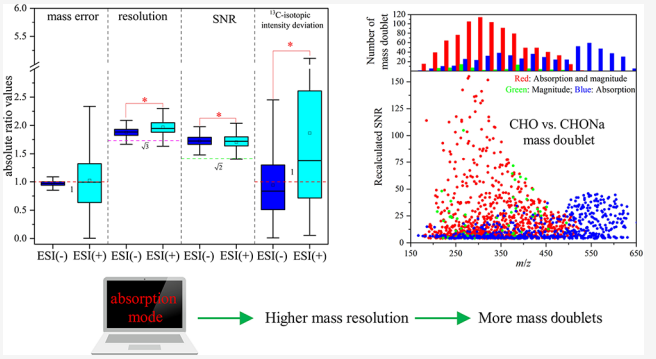

INTRODUCTION

Ultrahigh resolution is a vital feature of Fourier transform ion cyclotron resonance mass spectrometry (FT-ICR MS) over other mass spectrometry techniques, enabling its capacity of resolving thousands of ions at subparts per million levels for organic mixtures, including dissolved organic matter (DOM). The resolution of FT-ICR MS is theoretically proportional to the strength of high-field superconducting magnets but inverse to the m/z value, resulting in the inferior performance of FT-ICR MS toward high m/z (*e.g.*, > 500).[1,2] Furthermore, the mass accuracy and resolution of FT-ICR MS spectra could be improved mainly by the internal calibration,[3] peak alignment,[4] and phasing of the raw FT-ICR MS data[5] during postdata processing.

The absorption mode of FT-ICR MS spectra had been recognized to afford higher resolution than the conventional magnitude mode of FT-ICR MS spectra when the Fourier transform was first introduced to ICR MS spectrometry.[6] The improvement factors were theoretically estimated as 1.4−2 depending on the system pressure and collision dynamics.[7−9] In addition to mass resolution, compared to the magnitude mode, the absorption mode is capable of[1] improving the signal-to-noise ratio (SNR) by a theoretical factor of $\sqrt{2}$,[2] improving mass accuracy,[3] decreasing the intensity deviation of isotopic peaks over two folds,[4] minimizing artifact peaks from harmonics and radio frequency interference,[5] retaining true peaks that often occur in the magnitude-mode spectra, and[6] identifying new peaks that do not appear in the magnitude-display spectra.[5−8,10−12] Initially, the absorption mode was only effective for a narrow spectral bandwidth, requiring interinteractive "turning" to perform the phase correction.[6,9] Then, the first successful broadband application of the absorption to the organic mixtures without user interactions was achieved by the simultaneous excitation and detection methods for ions, with the ion cyclotron radial less than half of the trapped-ion cell radius.[13] Because of the different initial phase angles and time delay (approximately 1 ms) between excitation and detection, the first automated broadband phase correction was developed for all peaks in the FT-ICR MS spectra of complex mixtures in 2010,[12] followed by the establishment of an empirical phase-correction method using a quadratic least-squares fitting.[14] Since then, the absorption mode has been employed to characterize the molecular

Received: October 15, 2023
Revised: November 29, 2023
Accepted: December 7, 2023
Published: December 21, 2023

https://doi.org/10.1021/acs.analchem.3c04651
Anal. Chem. 2024, 96, 522−530

composition of petroleum, biological samples (*e.g.*, proteins, lipids, and monoclonal antibodies), lignins, and DOM.[5,11,15−22]

DOM is a complex mixture of thousands of organic compounds from the biotic and abiotic transformations of plant, animal, and microbial matter,[23] playing essential roles in various chemical and biogeochemical processes in the engineered systems and critical natural zones of surface Earth.[1] The ultrahigh mass resolution is essential to characterize the molecular composition of DOM because of its complex nature.[24] For the first time, the superiority of the absorption mode had been highlighted for the molecular characterization of DOM.[20] Both negative-ion and positive-ion electrospray ionization modes [ESI(−) and ESI(+), respectively] have been proposed to comprehensively elucidate the molecular composition of DOM as a result of the ionization preference of both charge modes.[22,25,26] The ESI(−)-FT-ICR MS spectra of DOM are complicated by the extensive occurrence of the cationic adducts, such as sodium-containing adducts (Na-adducts) and potassium-containing adducts (K-adducts),[22,26,27] which may not be separated satisfactorily from the neighbor ions at a high m/z range (*i.e.*, > 500) due to the inherent less mass resolutions at the high m/z range. Some mass doublets, such as C_2 versus H_1Na_1 [Δmass = 2.40 millidalton (mDa)] and H_5K_1 versus ON_2 (Δmass = 1.77 mDa), were often overlapped in the ESI(+)-FT-ICR MS spectra acquired by the 7 Telsa FT-ICR MS instrument. Therefore, adducts in the ESI(+)-FT-ICR MS spectra of DOM are expected to be better resolved by the absorption mode than the magnitude mode, particularly for mass doublets in the high m/z range. However, the improved FT-ICR MS spectra of DOM by the absorption mode has been previously highlighted for the spectra only operated in the identical charge mode.[20−22] There is still no study comparing the spectral improvement by the absorption mode for the same DOM sample ionized between the ESI(−) and ESI(+) modes.

In this study, three typical DOM [Suwannee River natural organic matter (SRNOM), leonardite humic acid (LHA), and lake DOM] were employed to compare the absorption mode-derived spectral improvement (*e.g.*, the number of assigned peaks, mass accuracy, intensity deviation of ^{13}C-isotopic peaks, SNR, and resolution) for FT-ICR MS spectra measured in the ESI(−) mode with the ESI(+) mode by a low-field (7 Telsa) FT-ICR MS instrument. Moreover, this improvement is also compared for the ESI(−)-FT-ICR MS spectra with the ESI(+)-FT-ICR MS spectra of the soil DOM measured by a 21 Telsa FT-ICR MS instrument. The findings of this study are expected to highlight the superiority of the absorption mode for the ESI(+)-FT-ICR MS spectra over ESI(−)-FT-ICR MS spectra.

EXPERIMENTAL SECTION

Sample Preparation. The SRNOM (2R101N) and LHA (1S104H) purchased from the International Humic Substance Society were completely and partially dissolved in methanol separately (LC-MS grade). The lake DOM (hereafter referred to as ELDOM) was extracted from the East Lake water of Wuhan City, China, using the method described elsewhere.[28,29] Briefly, lake water (1 L) was filtered with a 0.45 μm membrane and acidified to pH ∼ 2 using concentrated HCl (Guaranteed grade), followed by the solid-phase extraction using the Bond Elut PPL cartridge (500 mg 6 mL, Agilent, USA) rinsed and activated with methanol (HPLC-MS grade, Thermo Fisher, USA) and diluted HCl (pH ∼ 2). The cartridge was desalted with 50 mL of diluted HCl and 5 mL of deionized water, thoroughly dried with N_2 gas, and eluted with methanol. All DOM solutions were diluted with methanol and deionized water to the desired concentrations. The diluted DOM in the 50% methanol (v: v) was refiltered with a 0.22 μm membrane to remove particles before the FT-ICR MS measurement completely.

FT-ICR MS Measurement. The FT-ICR MS spectra of the three DOM samples were analyzed using the FT-ICR MS instrument equipped with a 7 Telsa superconducting magnet and a quadrupole detector (SolariX 2XR, Bruker Daltonics, Bremen, Germany) in the magnitude mode at the China University of Geosciences, Wuhan. The magnitude mode data were later processed to the absorption mode data (see the next section). The FT-ICR MS spectra were optimized with our previously reported spectral quality assessment strategy[30] and acquired in both ionization modes with the following parameters: 4200 V and 5000 capillary voltage for the ESI(−) and ESI(+) modes, respectively; 120 μL/h direct infusion rate; 4MWord data size; 1000 average scans; 0.007 and 0.100 s ion accumulations for the ESI(−) and ESI(+) modes, respectively; 107−1000 mass-to-charge ratio (m/z) range; −3.0 and 3.0 V front and back trap plate voltage for the ESI(−) and ESI(+) modes, respectively; and 0.7 s time-of-flight. Both ESI(−)-FT-ICR MS and ESI(+)-FT-ICR MS spectra were externally calibrated with the sodium trifluoroacetate standard [10.0 and 100 mg/L for the ESI(−) and ESI(+) modes, respectively].

Moreover, the ESI(−)-FT-ICR MS and ESI(+)-FT-ICR MS spectra of a pyrogenic soil DOM (PSDOM) in both magnitude and absorption modes were obtained from the Open Science Framework (OSF) at https://osf.io/758ux/ (DOI: 10.17605/OSF.IO/758UX). A high-field (21 Telsa) FT-ICR MS instrument in the national high magnetic field laboratory at the Florida State University, USA, was employed to measure the PSDOM sample in both ionization modes.[22]

Data Processing. The raw FT-ICR MS data (free induction decay (FID) signal) were phased-corrected with the instrument software, namely, FTMS Processing (version 2.3.0, Bruker Daltonics, 2019), according to the software tutorial (Figure S1). Briefly, the spectra were apodized with the half-sine function. The absorption mode processing (AMP) parameters were set as 0, 100, and 1000 for AMP center, and low and high masses, respectively; 25 AMP minimum peak SNR. The spectral phase was then fitted with a default genetic algorithm. Baselines of the phased absorption display of FT-ICR MS spectra were corrected with the "Simple_100" method, which minimizes the fluctuation of noise peaks arising from the phase correction. All FT-ICR MS spectra of the SRNOM, ELHA, and ELDOM in the magnitude and phase-corrected absorption modes were further internally calibrated using the known-CHO series obtained from the FT-ICR MS spectrum of SRNOM.

All phase-corrected (only for the absorption mode) and internally calibrated FT-ICR MS spectra (m/z = 100−1000) of the PSDOM available at the OSF depository were subsequently subjected to the formula assignment without any additional processing. The chemical formulas for all FT-ICR MS spectra in the magnitude and absorption modes were assigned using the FTMSDeu algorithm[31] with the following computation conditions: (i) SNR ≥ 4 and 6 for non-halogenated and halogenated monoisotopic formulae, respec-

https://doi.org/10.1021/acs.analchem.3c04651
Anal. Chem. 2024, 96, 522−530

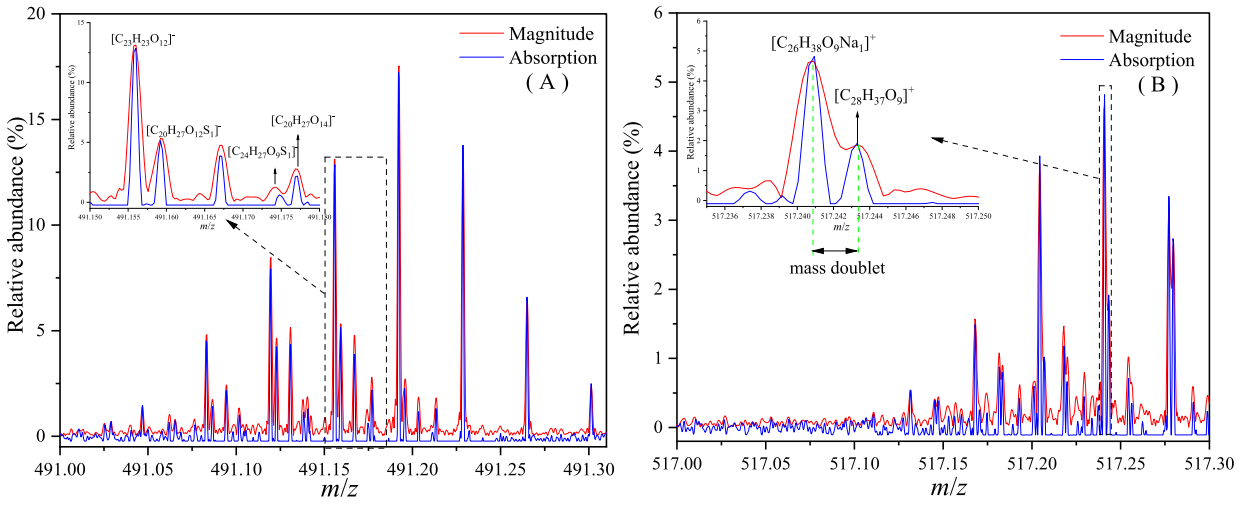

Figure 1. Enlarged FT-ICR MS spectra of ELDOM: (A) at a nominal mass of 491 in the ESI(−) mode and (B) at a nominal mass of 517 in the ESI(+) mode.

tively; (ii) $0.3 \leq (H + Cl + Br)/C \leq 2.25$ and $0 < O/C \leq 1.2$ for molecules with $C \geq 5$ for the ESI(−) mode; (iii) $0.3 \leq (H + Cl + Br)/C \leq 4$ and $0 \leq O/C \leq 1.2$ for molecules with $C \leq 4$ for the ESI(−) mode; (iv) $0.3 \leq (H + Cl + Br)/C \leq 4$ and $0 \leq O/C \leq 1.2$ for the ESI(+) mode; (v) an integer value ≥ 0 for double-bond equivalent (DBE); (vi) $1 \leq {}^{12}C \leq 50$, ${}^{13}C \leq 2$, ${}^{18}O \leq 1$, ${}^{14}N \leq 5$, ${}^{15}N \leq 1$, ${}^{32}S \leq 3$, ${}^{33}S \leq 1$, ${}^{34}S \leq 1$, $P \leq 1$, ${}^{35}Cl \leq 5$, ${}^{37}Cl \leq 5$, ${}^{79}Br \leq 5$, ${}^{81}Br \leq 5$; (vii) $-10 \leq$ DBE-O ≤ 10 for the ESI(−) mode and $-13 \leq$ DBE-O ≤ 13 for the ESI(+) mode; (viii) Na + K = 1 or 2 for cationic adducts in the ESI(+) mode; (ix) a maximum allowed mass error of 1000 and 150 ppb for FT-ICR MS data collected by the low-field and high-field FT-ICR MS instruments, respectively; (x) maximum acceptable intensity deviations of isotopic peaks compared with their theoretical values were 30%, 50%, and 80% for theoretical relative abundance (RA) > 10%, 5%−10%, and ≤ 5%, respectively. According to the compositional space in the van Krevelen diagrams, assigned formulas were classified into nine classes.[26,29]

The SNR values of low-field FT-ICR MS spectra provided by the instrument Compass DataAnalysis software (version 5.0, Bruker Daltonics, 2017) were calculated based on the standard deviation of the third derivative values of the intensity of noise peak, i.e., the values do not necessarily indicate the intensity ratio of analyte peaks to noise peaks (Figures S2 and S3). The SNR values were therefore recalculated using an in-house MATLAB script described in Content S1 by directly dividing the intensity of each analyte peak at each nominal mass by the mean value of absolute intensities of all selected noise peaks at the corresponding nominal mass (Figure S2). The molecular parameters [such as modified aromaticity index (AI_{mod}), the nominal oxidation state of carbon (NOSC), and DBE], chemical classes, and elemental composition were calculated using the equations and criteria described elsewhere.[26]

For the statistical analysis, a one-way analysis of variance (ANOVA) was employed to statistically test the significant difference at $p < 0.05$ for variables that passed the normality test. Otherwise, the nonparametric Kruskal−Wallis one-way ANOVA was used. Formulas assigned in both magnitude-mode and absorption-mode spectra for the same sample were used to calculate the ratios of the resolution, SNR, mass error, and intensity deviation of ${}^{13}C$-isotopic peaks (if identified) in the absorption-mode spectra relative to those for the magnitude-mode spectra after excluding outlier data. Statistical analysis was conducted using MATLAB (version 2022b, MathWorks, USA) with the license no. in Content S2.

RESULTS AND DISCUSSION

Improved Performance for Low-Field Magnet Instrument. All FID-based FT-ICR MS raw data were phase-corrected using the FTMS Processing software with genetic algorithm scores of 0.965−0.972 and 0.953−0.970 for FT-ICR MS spectra in ESI(−) and -FT-ICR MS for ESI(+) modes, respectively, which were higher than the threshold value (0.8) suggested by the software tutorial. Compared with the magnitude mode, the angular frequency is exclusively considered in the absorption mode during Fourier transform processing of the frequency domain data for all excited ions in the ICR cell. The angular frequency will narrow the peak widths, thus providing higher peak resolutions in the absorption mode than in the magnitude mode.[5,12] Although the resolution of FT-ICR MS peaks reciprocally decreased with increasing m/z values ($R^2 = 0.780 - 0.880$, $P < 0.05$), its values were obviously improved in the entire absorption-display FT-ICR MS spectra (Figures S4). Therefore, the absorption mode display yields a narrower peak width than the magnitude mode, resulting in more peaks identified at larger m/z than those at low m/z[13,19] (Figure 1). For example, the mass doublets of $[C_{23}H_{23}O_{12}]^-$ versus $[C_{20}H_{27}O_{12}S_1]^-$ (C_3 versus H_4S_1, Δm = 3.37 mDa, and ΔDBE = 5) and $[C_{24}H_{27}O_9S_1]^-$ versus $[C_{20}H_{27}O_{14}]^-$ (O_5 versus C_4S_1, Δm = 2.50 mDa, and ΔDBE = 4) in the ESI(−)-FT-ICR MS spectra of the ELDOM were separated entirely in the absorption mode but only partially for the magnitude mode (Figure 1A). The protonated peak of $[C_{28}H_{37}O_9]^+$ was profoundly overlapped by the Na-adduct peak of $[C_{26}H_{38}O_9Na_1]^+$ in the ESI(+)-FT-ICR MS spectrum of the ELDOM in the magnitude mode and newly identified by the absorption mode (Figure 1B).

For formulas identified in both magnitude and absorption modes, the mean resolution ratio values for peaks in the absorption mode relative to the magnitude mode were 1.88 −1.91 and 1.88 −1.94 for ESI(−)-FT-ICR MS and ESI(+)-FT-ICR MS spectra of DOM collected by the 7 Telsa FT-ICR

https://doi.org/10.1021/acs.analchem.3c04651
Anal. Chem. 2024, 96, 522−530

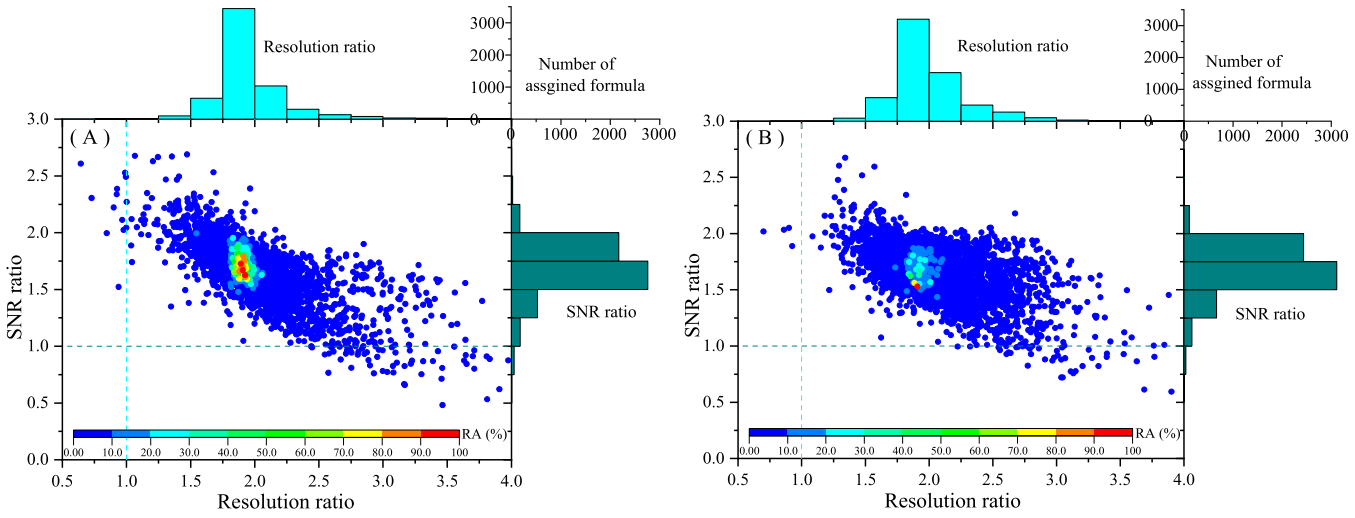

Figure 2. Scatter diagraph of the resolution against SNR ratios of common formulae in the absorption-display spectra relative to those for the magnitude-display spectra for ELDOM. (A): ESI(−)-FT-ICR MS spectra; (B): ESI(+)-FT-ICR MS spectra. The scatter color indicates the RA values of the formulae in the magnitude-display spectra.

MS instrument, respectively. The mean resolution ratio values highly approach the theoretical values of $\sqrt{3}$ and 2, corresponding to a pressure-limited Langevin collision mode (ion/induced dipole interaction) and zero pressure-limited mode (no ion collision), respectively.[9] Moreover, the resolution ratios of nearly all peaks (number percentage ≥ 99.8%) assigned in both magnitude and absorption modes were larger than 1 with its histogram center, and the resolution ratio for high-intensity peaks was around 1.9 (Figures 2, S5, and S6). These results have highlighted the improved resolutions for nearly all common formulas by the absorption mode, particularly for high-intensity peaks.

Improved SNR Ratios. The peak width in the absorption display is generally narrower than that for the identical peak in the magnitude display, resulting in higher SNR values for the FT-ICR MS peaks in the absorption display. Analogous to the resolution ratio, the SNR ratios (defined as the ratio of the recalculated SNR value for a given FT-ICR MS peak in the absorption mode relative to that for the identical peak in the magnitude mode) were averaged at 1.64−1.72 and 1.60−1.72 for the ESI(−)-FT-ICR MS and ESI(+)-FT-ICR MS spectra of DOM, which were slightly higher than the theoretical value ($\sqrt{2}$). The histogram center of SNR ratios for all formulas and formulas with high abundances generally ranged from 1.5 to 2.0 (Figures 2, S5, and S6), indicating that the SNR values of high-intensity peaks were improved by factors slightly higher than the theoretical value in this study. In addition to eliminating random errors in the imaginary axis,[5] the improvement of SNR ratios by the absorption mode could be mainly attributed to the additional baseline correction of the AMP processing. For example, the baseline correction treatment improved 21.9% and 24.6% of SNR values for the absorption displays of ELDOM in the ESI(−) and ESI(+) modes, respectively (Figure S7). The SNR ratios of peaks in the absorption displays of ELDOM without baseline correction were averaged at 1.39 and 1.36 for the ESI(−) and ESI(+) modes, respectively, which were highly close to the theoretical value but significantly lower ($P < 0.05$) than those for the baseline-corrected absorption displays (Figure S8). Moreover, the half-window apodization function (*e.g.*, the half-sine function) used in the AMP processing could partially contribute to the additional improvement of SNR values (compared to the theoretical improvement) because the signal at the beginning of the transient was expected to be suppressed by a full-window apodization function (*e.g.*, sine function) in the magnitude spectra. In contrast, the signal at the beginning of the transient could not be affected by the half-window apodization function in the absorption spectra using the half-sine function.[5]

Mass Accuracy and Intensity Deviation of ^{13}C-Isotopic Peaks. Overall, the absolute values of mass errors for internally calibrated peaks in the absorption mode slightly decreased from 26.6% to 21.7% for the ESI(−) mode and from 19.3% to 14.6% for the ESI(+) mode. These marginal mass accuracy improvements were slightly lower than those for the calmodulin (23%−64%)[5] but close and even better than those for crude oil (10%−24%), multiply charged ubiquitin (1%), and vacuum gas oil (21%).[12,32,33] However, for peaks commonly assigned in the magnitude and absorption displays, significantly lower ($P < 0.05$) absolute mass errors were observed in the absorption-display spectra than those for the magnitude-display spectra in both ionization modes (Figure S9). The mass accuracy improvement by the absorption mode could be mainly explained by the effects of phase correction on peak intensities, leading to changes in the peak picking by the Bruker Compass DataAnalysis software (version 5.2, 2019).[33]

Theoretically, the phase-dependent anomalous mass shift is expected for two closely spaced magnitude peaks closer than $3/T$ (T = acquisition time) because of the nonadditive nature of the magnitude spectra. However, it could be obviated by the phase correction in absorption display.[34] The mass accuracy of well-resolved FT-ICR MS peaks is proportional to the SNR values and the square root of the number of data points per peak width at half-maximum peak height (FWHM).[9,35] The mass accuracy of high-intensity peaks in the magnitude mode could be well-centroided and offset by their large FWHM, thus not significantly changed by the absorption mode.[5,9] In this study, the mass accuracy of the internally calibrated spectra in the magnitude mode was mainly less than 200 ppb (Figure S9), resulting in high absolute values of the mass error ratio for the magnitude-display FT-ICR MS spectra relative to those for the absorption mode. As depicted in Figures S10−S13, the

https://doi.org/10.1021/acs.analchem.3c04651
Anal. Chem. 2024, 96, 522−530

formulas with large mass error (≥200 ppb), accounting for the majority (72.3% ± 11.8% and 76.5% ± 3.5% for ESI(−) and ESI(+) modes, respectively) of identified formulas in the magnitude-display FT-ICR MS spectra, generally had absolute values of mass error ratio lower than 1 and significantly lower ($P < 0.05$) than those for formulas with small mass error (<200 ppb). This observation can be explained by the fact that the absorption display can improve the SNR values of low-SNR peaks, yielding higher mass accuracy for these peaks.[5,36]

Similarly, the intensity deviation ratio of the ^{13}C-intensity deviation for the assigned ^{13}C-isotopic formula in the absorption-display FT-ICR MS spectra relative to that for the magnitude-display FT-ICR MS spectra was also dependent on the absolute intensity deviation of the assigned ^{13}C-isotopic formula in the magnitude-display FT-ICR MS spectra (Figures S14−S16). The absolute values of the intensity deviation ratio for ^{13}C-isotopic formulas with large intensity deviation (≥10%) in the magnitude display were mainly lower than 1 and also significantly ($P < 0.05$, except for the ESI(+)-FT-ICR MS spectra of LHA) lower than those for ^{13}C-isotopic formulas with low-intensity deviation (<10%). These results suggest that the absorption mode can significantly improve the mass accuracy for DOM peaks with large mass errors and decrease the intensity deviation of ^{13}C-isotopic formulas with a large intensity deviation. In contrast, this technique showed minor positive improvements for DOM peaks with small mass errors and ^{13}C-isotopic formulas with low-intensity deviation.

Peak Detection and Formula Assignment. Overall, a considerable number of peaks in the magnitude-display FT-ICR MS spectra of DOM [46%−62% and 47%−57% for the ESI(−) and ESI(+) modes, respectively] were also detected in the corresponding absorption-mode spectra. Peaks detected in the absorption display accounted for 74%−91% of the total intensity for the magnitude display. In contrast, those common peaks accounted for 85%−96% and 94%−98% of the peak number and total intensity for each absorption-display FT-ICR MS spectrum, respectively. These results could be explained by the fact that all high-intensity peaks were detected in both magnitude-display and absorption-display spectra for each DOM sample. Moreover, the absorption display decreased the number of peaks by 27%−52% compared to the magnitude display but slightly affected the total intensity. The decreased peak number was partially caused by artifacts (*i.e.*, side-lodes for the ELDOM in Figure S17) in the magnitude-display spectra, in which the sine function could not be phased correctly due to their anomalous phase.[32] The proper resolve of side-lodes by the absorption mode will be favorable to identifying low-intensity peaks, particularly for some micropollutants in natural aquatic systems (*e.g.*, perfluoro-1-butane sulfonate, $[C_4F_9O_3S_1]^-$, and acetaminophen, $[C_8H_{10}N_1O_2]^+$, in the ELDOM Figure S18). Moreover, because the SNR and resolution values of low-intensity peaks are susceptible to noise, phase correction will amplify the variations in the SNR and resolution ratios of low-intensity peaks. For example, the coefficient of variation of the SNR and resolution ratios for low-intensity peaks were 2.67−3.25 folds of those of high-intensity peaks (Figures S19 and S20). Therefore, some peaks were detected only in the absorption-display or magnitude-display spectra.

Although the total number of detected peaks in the magnitude-display FT-ICR MS spectra of DOM was significantly higher ($P < 0.05$) than that for the absorption-display FT-ICR MS spectra in both ionization modes, the number of peaks assigned in the magnitude mode was 73%−89% and 70%−75% of that for the absorption mode in the ESI(−) and ESI(+) modes, respectively. Consequently, the formula assignment ratio (defined as the ratio of assigned peak number relative to the total detected peak number in a given spectrum) was increased in the absorption mode with factors of 1.9−2.2 for the ESI(−) and 1.8−12.9 for ESI(+). Chemical formulas were only assigned to peaks with SNR ≥ 4 in this study. The formula assignment ratio of the magnitude display was significantly lower ($P < 0.05$) than that for the absorption display because of the overwhelmingly higher ($P < 0.05$) proportion of low-SNR peaks (i.e., SNR < 4) in the magnitude display FT-ICR MS spectra than that for the absorption mode (49.2%−61.1% versus 1.2%−13.3% and 4.0%−14.0% versus 53.7%−67.2% for the ESI(−) and ESI(+) modes, respectively). Accordingly, this significant discrepancy in low-SNR peaks contributed to the observation that the number of peaks only assigned in the absorption display were 2.4- to 6.3-folds and 5.3- to 17.2-folds compared to those for the magnitude display in ESI(−) and ESI(+) modes (Table S1), respectively.

Specifically, monoisotopic peaks without and with ^{13}C-isotopic peaks accounted for 77% and 23% of the total formula number for the absorption-display spectra of ELDOM assigned only in the ESI(−) mode, respectively. Similar values were obtained for the ESI(+) mode (87% and 13% of the total formula number, respectively). Except for 21 and 35 formulas invalidated by the ^{13}C-isotopic pattern in both ionization modes, monoisotopic peaks for most other halogen-free formulas assigned were exclusively detected in the magnitude-display spectra (Table S1). In addition to halogen-free formulas, more halogen-containing formulas validated by the ^{37}Cl- or ^{81}Br-isotopic pattern were identified in the absorption-display spectra than the magnitude-display spectra. Regarding a few peaks with similar masses yet assigned to different formulas in both ionization modes, more halogen-containing formulas validated by the ^{37}Cl- or ^{81}Br-isotopic pattern were identified in the absorption-display spectra than in the magnitude-display spectra. Moreover, a moderate number of identical peaks were observed to be assigned to different halogen-free formulas in the magnitude-display and absorption-display spectra in the ESI(+) mode. These results could be mainly caused by the reasons discussed in Content S3 (Figure S21) and revealed that the absorption mode affected more the formula assignment of ESI(+)-FT-ICR MS spectra than the ESI(−)-FT-ICR MS spectra due to the occurrence of cationic adducts in the ESI(+)-FT-ICR MS spectra.

Indeed, the adduct formulas only assigned in the absorption-display spectra were 4.4−22 folds of those for the magnitude-display spectra (Figure S22). Furthermore, as illustrated in Figure S23, much less cationic adduct formulas were assigned exclusively to high-m/z peaks in the magnitude mode than in the absorption mode due to the inferior mass resolution and lower SNR values, particularly for peaks at high m/z. For example, the number of cationic adduct formulas assigned to peaks with $m/z > 600$ in the absorption-display spectra was 14−47 folds of those for the magnitude-display spectra. The absorption mode improved the resolutions and SNR values for all peaks, including $m/z \geq 500$ peaks, yielding more adducts only identified in absorption-display spectra at high m/z.

Superior Improvement of the Absorption Mode for ESI(+) over ESI(−). The mean and medium values of resolution ratio for ions commonly identified in both ionization modes were all in the range from $\sqrt{2}$ to 2, indicating that the ion cyclotron

https://doi.org/10.1021/acs.analchem.3c04651
Anal. Chem. 2024, 96, 522−530

radius for these compounds in both two charge modes remained constant (zero-pressure limit) or decreased exponentially with time during the data acquisition period (Langevin collision mode).[9] Similarly, the mean and medium values of the SNR ratio for these ions were all above the theoretical value. The resolution ratio and SNR ratio for the ESI(−)-FT-ICR MS spectra were significantly lower and higher ($P < 0.05$) than those for the ESI(+)-FT-ICR MS spectra, respectively (Figure S24). This result suggests the lower and higher improvement extents of resolution and SNR by the absorption mode for the ESI(−)-FT-ICR MS spectra than those for the ESI(+)-FT-ICR MS spectra, respectively. However, inconsistent tendency among different DOM samples was observed for the absolute ratios of mass error and ^{13}C-isotopic intensity deviation of commonly assigned peaks in both the charge modes (Figure S24), suggesting the different improvement extents by the absorption mode to the mass accuracy and ^{13}C-isotopic intensity deviation for the different FT-ICR MS spectra in both charge modes.

Because of the more abundant nature of ELDOM in the compounds with nonoxygen heteroatoms, including N and S, more N- or S-related isobaric overlaps were identified in the ELDOM than in the SRNOM and LHA (Tables S2 and S3). For example, the number of the H_4S_1 versus C_3 mass doublet (Δmass = 3.37 mDa and ΔDBE = 5) resolved in the ESI(−)-FT-ICR MS spectrum of ELDOM was 2.3- and 5.5-folds of that for the SRNOM and LHA, respectively. Furthermore, there were 111 mass doublets of N_3 versus $C_1{}^{13}C_1H_1O_1$ (Δmass = 3.13 mDa and ΔDBE = 0) in the ESI(−)-FT-ICR MS spectrum of ELDOM, contrasting with the absence of this mass doublet in the SRNOM and ELHA. The number of resolved H_4S_1 versus C_3 mass doublets was increased by the absorption mode to 141.0%, 225.0%, and 126.8% of the number for SRNOM, LHA, and ELDOM in the ESI(−) mode, respectively. For all three samples, the absorption mode-derived increase percentages for the total number of mass doublets resolved in the ESI(−) mode were significantly lower than those for the ESI(+) mode (113.2% ± 20.5% versus 150.1% ± 12.8%, $P < 0.05$), indicating the superiority of the absorption mode in resolving close mass doublets in the ESI(+) mode than the ESI(−) mode. Compared with the ESI(−)-FT-ICR MS spectra, the ESI(+)-FT-ICR MS spectra of DOM were featured in the extensive occurrence of close mass doublets,[27,37] which require higher resolutions to achieve satisfactory separations. For example, the mass doublet of Na-adduct and protonated ions due to the close mass difference between C_2 and H_1Na_1 (Δmass = 2.40 mDa and ΔDBE = 3, the mass doublet exemplified in Figure 1B) were detected in the ESI(+)-FT-ICR MS spectra of DOM from m/z 150 to 650 (Figures 3, S25, and S26). In total, 26.0%−38.0% number of all assigned formulae in the magnitude-display spectra of SRNOM, LHA, and ELDOM were identified as Na-adducts, which was higher than that for PSDOM.[22] The number of this mass doublet in the absorption-display spectra was higher than that in the magnitude-display spectra, particularly for the peak pairs at high m/z ($m/z > 500$). As exemplified in Figure 1, unresolved peak pairs at high m/z could be satisfactorily identified by the absorption mode, yielding more mass doublet exclusively assigned in the absorption-display spectra due to its capacity of improving mass resolution (blue scatters and columns in Figures 3, S25, and S26). Moreover, compared with the magnitude mode, the absorption mode increased the number of another Na-adduct-related mass doublet,

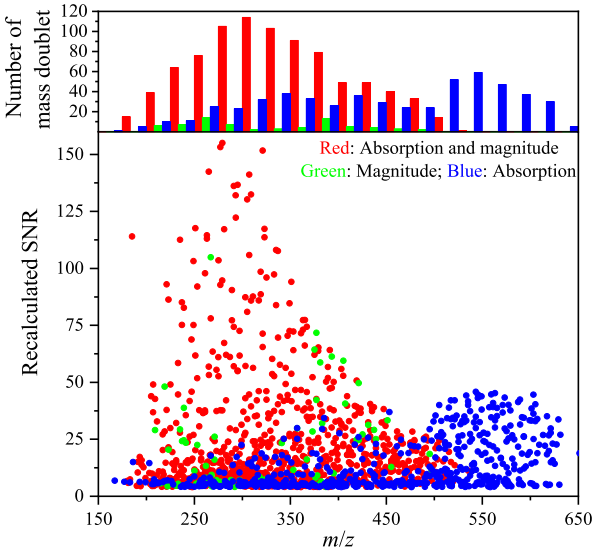

Figure 3. Scatter digraph of m/z against recalculated SNR values (down) and histogram of m/z value for the mass doublet of Na-adduct and protonated peaks in the absorption-display and magnitude-display spectra for ELDOM. Red scatter and column indicate this mass doublet assigned in both magnitude and absorption modes; green scatter and column indicate this mass doublet assigned exclusively in the magnitude mode; blue scatter and column indicate this mass doublet assigned exclusively in the absorption mode. Recalculated SNR values in the magnitude mode were used for peak doublets assigned in both the magnitude and absorption modes.

$^{13}C_1H_2Na_1$ versus C_2N_1 (Δmass = 5.70 mDa and ΔDBE = 3), by 0.5−2.6 folds (Tables S4 and S5). Moreover, except for the LHA rich in condensed aromatics, both SRNOM and ELDOM were mainly composed of lignins and tannins (Table S6). The intensity percentage ratios of condensed aromatics, lignins, and tannins in the absorption mode relative to those in the magnitude mode were averaged at 1.06 ± 0.17, 1.01 ± 0.02, and 0.95 ± 0.12 for the ESI(−)-FT-ICR MS spectra, respectively, which were not significantly different from those values (1.20 ± 0.16, 1.00 ± 0.02, and 1.09 ± 0.31, respectively, $P > 0.05$) for the ESI(+)-FT-ICR MS spectra. Moreover, intensity percentage ratios of different elemental classes (e.g., CHO, CHON, and CHOS) and intensity-weighted ratios of molecular parameters (*e.g.*, m/z_{iw}, O/C_{iw}, H/C_{iw}. $AI_{mod,iw}$, DBE_{iw}, and $NOSC_{iw}$) in the absorption-display spectra relative to those for the magnitude-display spectra tabulated in Table S7 were averaged at 0.97 ± 0.09 and 0.98 ± 0.02 in the ESI(−) mode, respectively, which differentiated insignificantly from those for the ESI(+)-FT-ICR MS spectra (1.00 ± 0.06 and 1.01 ± 0.02, respectively, $P > 0.05$). Those results suggest the overall minor effects of the absorption mode on the molecular composition of DOM in both charge modes. Therefore, the absorption mode is recommended for the ESI(+)-FT-ICR MS spectra of DOM because of its great potential in resolving the cationic adduct peaks from adjacent protonated peaks, particularly for high m/z peaks.

Comparison of the Absorption Mode for High-Field Magnet Instrument. Similarly to the 7 Telsa FT-ICR MS instrument, the mass resolution of 21 Telsa FT-ICR MS peaks in absorption-display and magnitude-display spectra reciprocally decreased with the increasing m/z values in both charge modes (R^2 = 0.490− 0.838, $P < 0.05$, Figure S27). The absorption mode exhibited minor effects on the molecular

https://doi.org/10.1021/acs.analchem.3c04651
Anal. Chem. 2024, 96, 522−530

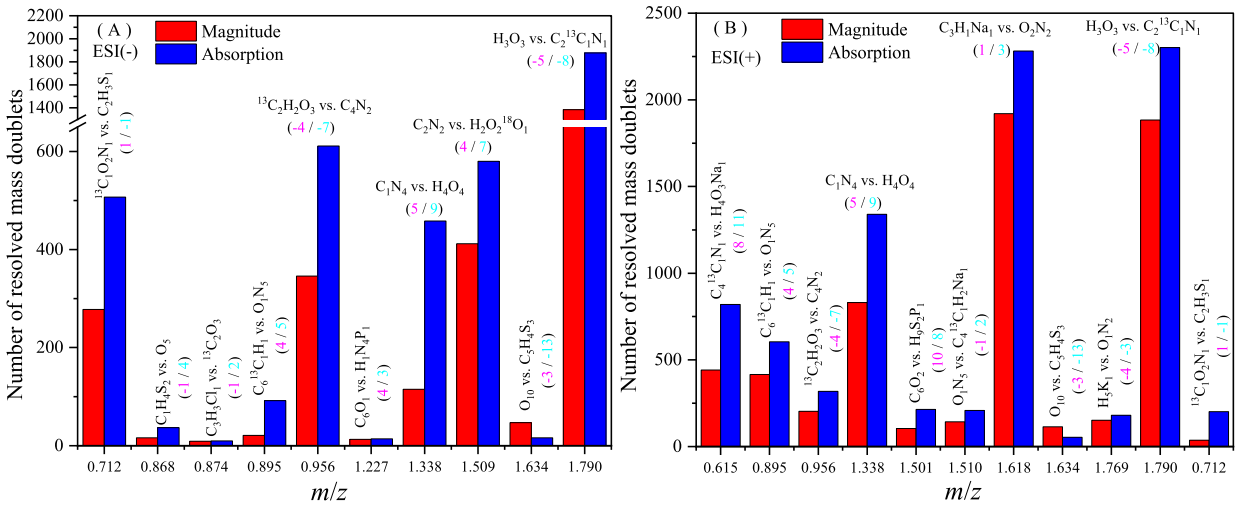

Figure 4. Mass doublets within 2 mDa resolved by 21 Telsa ESI(−)-FT-ICR MS (A) and ESI(+)-FT-ICR MS (B) in the magnitude and absorption modes. Magenta and cyan numbers in the bracket indicate DBE and DBE minus oxygen values for the elemental composition on the left side minus those on the right side of mass doublets.

classes, elemental composition, and molecular properties of PSDOM in both ionization modes (Tables S6 and S7). The number of detected PSDOM peaks in the same mode by the high-field magnet instrument was approximately 3- to 4-fold of those for our low-field magnet instrument, mainly because of the profound higher resolution of 21 Telsa FT-ICR MS instrument (*e.g.*, ∼1,800,000 at *m*/*z* 400) than our 7 Telsa FT-ICR MS instrument (e.g. ∼330,000 at *m*/*z* 400).[22] The SNR values of nearly all common formulas [94.5 and 99.5% for ESI(−) and ESI(+) modes, respectively] in the PSDOM were significantly enhanced by the absorption mode ($P < 0.05$), particularly for high-intensity peaks (Figure S28). Similar to the improved performance for the FT-ICR MS spectra acquired by the low-filed magnet, the averaged SNR and resolution ratio values (1.3 and 1.6, respectively) were both close to the theoretical values of $\sqrt{2}$ and $\sqrt{3}$ to 2.0, respectively. Despite the unprecedented resolution of the 21 Telsa FT-ICR MS instrument, the enhanced resolutions by the absorption mode eventually facilitate the separation of significant mass doublets, yielding more formulas detected and assigned than those in the magnitude mode [*e.g.*, 43,023 versus 38,473 and 38,177 versus 32,379 for detected and assigned peaks in the ESI(+) mode, respectively]. In total, the magnitude mode of 21 Telsa FT-ICR MS resolved 2698 and 6717 mass doublets within a mass difference of 2 mDa in the ESI(−) and ESI(+) modes, respectively, while the absorption mode increased the corresponding numbers to 4431 and 9307, respectively. The occurrence of Na-related adducts and preferential ionization of CHON molecules in the ESI(+) mode[22,26,27] mainly account for higher numbers of resolved mass doublets in this charge mode than in the ESI(−) mode. Indeed, compared with the magnitude display, more than 1000 CHONa and 3000 CHON ions were newly identified in the absorption-display spectra of PSDOM. The mass doublets of $^{13}C_1O_2N_1$ versus $C_2H_3S_1$ (Δmass = 0.71 mDa and ΔDBE = 1), $^{13}C_2H_2O_3$ versus C_4N_2 (Δmass = 0.96 mDa, and ΔDBE = 4), C_1N_4 versus H_4O_4 (Δmass = 1.34 mDa and ΔDBE = 5), C_2N_2 versus $H_2O_2{}^{18}O_1$ (Δmass = 1.51 mDa, and ΔDBE = 4), and H_3O_3 versus $C_2{}^{13}C_1N_1$ (Δmass = 1.79 mDa, and ΔDBE = 5) accounted for the majority (≥95%) of total and increased mass doublets resolved by the ESI(−)-FT-ICR MS (Figure 4A). For the ESI(+)-FT-ICR MS, the absorption mode was featured in obviously separating the major mass doublets including $C_4{}^{13}C_1N_1$ versus $H_4O_3Na_1$ (Δmass = 0.62 mDa, and ΔDBE = 8), $C_6{}^{13}C_1H_1$ versus O_1N_5 (Δmass = 0.90 mDa, and ΔDBE = 4), C_1N_4 versus H_4O_4 (Δmass = 1.34 mDa, and ΔDBE = 5), $C_3H_1Na_1$ versus O_2N_2 (Δmass = 1.62 mDa, and ΔDBE = 1), and H_3O_3 versus $C_2{}^{13}C_1N_1$ (Δmass = 1.79 mDa, and ΔDBE = 1) with ∼20 to ∼86% increase of mass doublet numbers (Figure 4B). Although the DBE discrepancy for resolved mass doublets indicated the possible overlapped compounds with different double bonds, only slight changes caused by the absorption mode were observed in the overall intensity-weighed parameters and intensity percentages of the compound and elemental classes (Tables S6 and S7). The mass differences of $^{13}C_1O_2N_1$ versus $C_2H_3S_1$ and $C_4{}^{13}C_1N_1$ versus $H_4O_3Na_1$ approximate the mass of an electron (0.548 mDa),[22] highlighting the great potential of the absorption mode and high-field magnet FT-ICR MS instrument for the identification of closely spaced mass doublets.[38] Although the absolute ratios of SNR and ^{13}C-isotopic intensity deviation were not significantly ($P > 0.05$) affected between ESI(−) and ESI(+) modes, significant ($P < 0.05$) decrease and increase by the absorption mode were observed for the absolute ratios of mass error and resolution between two charge modes, respectively (Figure S29). The FT-ICR MS resolution is much more profoundly improved by the absorption mode than by other FT-ICR MS spectral indices, including mass error, SNR, and ^{13}C-isotopic intensity deviation.

Environmental Implication. The high-throughput and nontarget analysis of environmental samples is highly challenged by their complex chemical compositions. The resolution of mass spectrometry is the critical factor affecting its high-throughput and nontarget analysis performance for extracts from various environmental matrices, such as aquatic DOM and soil-derived DOM. The superior resolution of the absorption mode over the conventional magnitude mode enables its additional identification for low-intensity peaks overlapped by adjacent high-intensity peaks with the mass differences in the sub-mDa to mDa levels, depending on the FT-ICR MS instrument performance. Differing from the slight changes in the formulaic results obtained by different

https://doi.org/10.1021/acs.analchem.3c04651
Anal. Chem. 2024, 96, 522−530

instruments,[39] the absorption mode-derived superior resolution is expected to be consistent for similar samples measured by different instruments. For example, no significant difference was observed in the ratios of intensity-weighed parameters and intensity percentages of elemental classes in the absorption mode relative to those for the magnitude between the SRNOM sample measured by our 7 Telsa FT-ICR MS and the PSDOM measured by 21 Telsa FT-ICR MS ($P > 0.05$, Figure S30). The additional identification is helpful in the high-throughput and nontarget analysis of fingerprint molecules in the DOM, which generally contains nonoxygen heteroatoms, such as sulfur-bearing surfactants (H_4S_1 versus C_3, Δmass = 3.37 mDa, ΔDBE = 5). This vital merit without additional economic cost is more significant for the ESI(+)-FT-ICR MS spectra of organic complex mixtures due to the extensive occurrence of mass doublets, such as CHO versus CHONa. The absorption mode will facilitate the FT-ICR MS-based complementary analysis of DOM because multiple ionization sources and ionization charge modes favor the complementary analysis of organic mixtures.[26,40,41]

Furthermore, FT-ICR MS peaks of the deuterium (D)-labeled DOM sample in the hydroxyl and/or carboxylic functional groups are frequently overlapped and require higher mass resolution to identify D-labeled peaks satisfactorily.[31,42,43] For example, as illustrated in Figures S31 and S32, the overlapped ESI(−)-FT-ICR MS peak series in the magnitude mode caused by mass doublets of $^{13}C_1H_1$ versus C_1D_1 (Δmass = 2.92 mDa, ΔDBE = 0) and D_2 versus H_4 (Δmass = 3.10 mDa, ΔDBE = 1) at nominal masses of 551 and 552 can be entirely separated by the absorption mode. Therefore, the narrower peak width of the absorption-display spectra will facilitate the elucidation of the chemical compositions and structure interpretations for overlapped FT-ICR MS peaks from highly complex mixtures, including DOM and petroleum.

CONCLUSIONS

This study has systemically compared the magnitude-display and absorption-display FT-ICR MS spectra of DOM acquired by the low-field and high-field magnet FT-ICR MS instruments in both ionization modes. For the 7 Telsa FT-ICR MS instrument, the raw DOM FT-ICR MS data were phase-corrected using the FTMS Processing software with genetic algorithm scores of more than 0.95. The resolution of DOM mass peaks in the absorption mode was enhanced by factors of 1.88−1.91 and 1.88−1.94 for ESI(−) and ESI(+) modes, respectively. The improvement factor for SNR values [1.64−1.72 for ESI(−) and 1.60−1.72 for ESI(+)] by the absorption mode was slightly higher than the theoretical value due to the additional baseline correction during the absorption-mode processing. Similarly, compared with the magnitude mode, the averaged SNR and resolution ratio values of DOM mass peaks by the 21 Telsa FT-ICR MS instrument in the absorption mode were (1.3 and 1.6, respectively) close to the theoretical values. For both low-field and high-field magnet FT-ICR MS instruments, the additional resolution in the absorption mode enables more formulas exclusively identified in the ESI(+) mode than in the ESI(−) mode due to the extensive occurrence of mass doublets with the mass differences in the sub-mDa to mDa levels in the ESI(+) mode. The findings of this study have systemically demonstrated the superiority of the absorption mode in improving the quality of FT-ICR MS spectra in the routine FT-ICR MS postdata analysis and highlighted its great potential in characterizing the molecular composition of DOM using the FT-ICR MS technique in both ESI(−) and ESI(+) modes.

ASSOCIATED CONTENT

Supporting Information

The Supporting Information is available free of charge at https://pubs.acs.org/doi/10.1021/acs.analchem.3c04651.

SNR recalculation; MATLAB license; reasons for differently assigned formulas; number of differently assigned formulas; mass doublet tables; intensity percentage of different classes, elemental classes, and molecular parameters; representative screenshot of phase correction; decreased resolutions with the increase of m/z; scatter digraph of resolution against SNR; SNR ratios; absolute mass error of common formulas; scatter and histogram diagraphs; absolute value of mass error ratio; absolute value of intensity deviation ratio of ^{13}C-isotopic formulas; representative side-lodes; enlarged FT-ICR MS spectra; SNR ratio variation; resolution ratio variation; formula number of adducted ions; absolute ratio values of mass error, resolution, SNR, and ^{13}C-isotopic intensity deviation; and ratios of elemental classes and molecular parameters All formula results and FT-ICR MS spectra for the 7 Telsa magnet instrument are freely available at 10.6084/m9.figshare.24602916.v1 (PDF)

AUTHOR INFORMATION

Corresponding Author

Qing-Long Fu − *MOE Key Laboratory of Groundwater Quality and Health, School of Environmental Studies, China University of Geosciences, Wuhan 430078, China;* orcid.org/0000-0002-7125-6877; Email: fuqinglong@cug.edu.cn

Authors

Chao Chen − *Guangdong Provincial Key Laboratory of Chemical Measurement and Emergency Test Technology, Institute of Analysis, Guangdong Academy of Sciences (China National Analytical Center, Guangzhou), Guangzhou 510070, China*

Yang Liu − *MOE Key Laboratory of Groundwater Quality and Health, School of Environmental Studies, China University of Geosciences, Wuhan 430078, China*

Manabu Fujii − *Department of Civil and Environmental Engineering, Tokyo Institute of Technology, Tokyo 152-8550, Japan;* orcid.org/0000-0001-7319-6014

Pingqing Fu − *Institute of Surface-Earth System Science, School of Earth System Science, Tianjin University, Tianjin 300072, China;* orcid.org/0000-0001-6249-2280

Complete contact information is available at: https://pubs.acs.org/10.1021/acs.analchem.3c04651

Notes

The authors declare no competing financial interest.

ACKNOWLEDGMENTS

The authors are grateful to Dr. Amy M. McKenna for providing 21 Telsa FT-ICR MS data. This study was financially supported by the National Natural Science Foundation of China (no. 42107484) and the Fundamental Research Funds

for the Central Universities, China University of Geosciences (Wuhan) (122-G1323522145).

REFERENCES

(1) Qi, Y.; Xie, Q.; Wang, J.-J.; He, D.; Bao, H.; Fu, Q.-L.; Su, S.; Sheng, M.; Li, S.-L.; Volmer, D. A.; et al. *Carbon Res.* **2022**, *1* (1), 3.
(2) Qi, Y. L.; Fu, P. Q.; Volmer, D. A. *Mass Spectrom. Rev.* **2022**, *41* (5), 647−661.
(3) Fu, Q. L.; Fujii, M.; Kwon, E. *Anal. Chem.* **2022**, *94* (30), 10589−10594.
(4) Merder, J.; Freund, J. A.; Feudel, U.; Niggemann, J.; Singer, G.; Dittmar, T. *Anal. Chem.* **2020**, *92* (3), 2558−2565.
(5) Qi, Y. L.; Barrow, M. P.; Li, H. L.; Meier, J. E.; Van Orden, S. L.; Thompson, C. J.; O'Connor, P. B. *Anal. Chem.* **2012**, *84* (6), 2923−2929.
(6) Comisarow, M. B.; Marshall, A. G. *Can. J. Chem.* **1974**, *52* (10), 1997−1999.
(7) Comisarow, M. B.; Marshall, A. G. *J. Chem. Phys.* **1976**, *64* (1), 110−119.
(8) Marshall, A. G.; Comisarow, M. B.; Parisod, G. *J. Chem. Phys.* **1979**, *71* (11), 4434−4444.
(9) Vining, B. A.; Bossio, R. E.; Marshall, A. G. *Anal. Chem.* **1999**, *71* (2), 460−467.
(10) Guan, S. H.; Li, G. Z.; Marshall, A. G. *Int. J. Mass Spectrom.* **1997**, *167*, 185−193.
(11) Qi, Y. L.; Li, H. L.; Wills, R. H.; Perez-Hurtado, P.; Yu, X.; Kilgour, D. P. A.; Barrow, M. P.; Lin, C.; O'Connor, P. B. *J. Am. Soc. Mass Spectrom.* **2013**, *24* (6), 828−834.
(12) Xian, F.; Hendrickson, C. L.; Blakney, G. T.; Beu, S. C.; Marshall, A. G. *Anal. Chem.* **2010**, *82* (21), 8807−8812.
(13) Beu, S. C.; Blakney, G. T.; Quinn, J. P.; Hendrickson, C. L.; Marshall, A. G. *Anal. Chem.* **2004**, *76* (19), 5756−5761.
(14) Qi, Y. L.; Thompson, C. J.; Van Orden, S. L.; O'Connor, P. B. *J. Am. Soc. Mass Spectrom.* **2011**, *22* (1), 138−147.
(15) Zhurov, K. O.; Kozhinov, A. N.; Fomelli, L.; Tsybin, Y. O. *Anal. Chem.* **2014**, *86* (7), 3308−3316.
(16) Kooijman, P. C.; Nagornov, K. O.; Kozhinov, A. N.; Kilgour, D. P. A.; Tsybin, Y. O.; Heeren, R. M. A.; Ellis, S. R. *Sci. Rep.* **2019**, *9*, 8.
(17) van der Burgt, Y. E. M.; Kilgour, D. P. A.; Tsybin, Y. O.; Srzentic, K.; Fornelli, L.; Beck, A.; Wuhrer, M.; Nicolardi, S. *Anal. Chem.* **2019**, *91* (3), 2079−2085.
(18) Vandergrift, G. W.; Kew, W.; Lukowski, J. K.; Bhattacharjee, A.; Liyu, A. V.; Shank, E. A.; Pasa-Tolic, L.; Prabhakaran, V.; Anderton, C. R. *Anal. Chem.* **2022**, *94* (8), 3629−3636.
(19) Qi, Y. L.; Luo, R. J.; Schrader, W.; Volmer, D. A. *Facets* **2017**, *2*, 461−475.
(20) Smith, D. F.; Podgorski, D. C.; Rodgers, R. P.; Blakney, G. T.; Hendrickson, C. L. *Anal. Chem.* **2018**, *90* (3), 2041−2047.
(21) Da Silva, M. P.; Kaesler, J. M.; Reemtsma, T.; Lechtenfeld, O. J. *J. Am. Soc. Mass Spectrom.* **2020**, *31* (7), 1615−1618.
(22) Roth, H. K.; Borch, T.; Young, R. B.; Bahureksa, W.; Blakney, G. T.; Nelson, A. R.; Wilkins, M. J.; McKenna, A. M. *Anal. Chem.* **2022**, *94* (6), 2973−2980.
(23) McKnight, D. M.; Aiken, G. R. Sources and Age of Aquatic Humus. In *Aquatic Humic Substances: Ecology and Biogeochemistry*, Hessen, D. O., Tranvik, L. J. Eds.; Springer: Berlin Heidelberg, 1998; pp. 9-39.
(24) Fievre, A.; Solouki, T.; Marshall, A. G.; Cooper, W. T. *Energy Fuels* **1997**, *11* (3), 554−560.
(25) Zhao, P. P.; Du, Z. L.; Fu, Q. L.; Ai, J.; Hu, A. B.; Wang, D. S.; Zhang, W. J. *Water Res.* **2023**, *232*, No. 119687.
(26) Zhou, Z. Q.; Fu, Q. L.; Fujii, M.; Waite, T. D. *Environ. Sci. Technol.* **2023**, *57* (11), 4690−4700.
(27) Koch, B. P.; Witt, M. R.; Engbrodt, R.; Dittmar, T.; Kattner, G. *Geochim. Cosmochim. Acta* **2005**, *69* (13), 3299−3308.
(28) Dittmar, T.; Koch, B.; Hertkorn, N.; Kattner, G. *Limnol. Oceanogr. Meth.* **2008**, *6*, 230−235.
(29) Fu, Q. L.; Fujii, M.; Kwon, E. *Anal. Chem.* **2020**, *92* (20), 13989−13996.
(30) Sun, J. J.; Liang, Y.; Fu, Q. L. *J. Am. Soc. Mass Spectrom.* **2023**, *34* (8), 1813−1820.
(31) Fu, Q. L.; Fujii, M.; Watanabe, A.; Kwon, E. *Anal. Chem.* **2022**, *94* (3), 1717−1725.
(32) Qi, Y. L.; Witt, M.; Jertz, R.; Baykut, G.; Barrow, M. P.; Nikolaev, E. N.; O'Connor, P. B. *Rapid Commun. Mass Spectrom.* **2012**, *26* (17), 2021−2026.
(33) Qi, Y. L.; Barrow, M. P.; Van Orden, S. L.; Thompson, C. J.; Li, H. L.; Perez-Hurtado, P.; O'Connor, P. B. *Anal. Chem.* **2011**, *83* (22), 8477−8483.
(34) Chow, K. H.; Comisarow, M. B. *Int. J. Mass Spectrom. Ion Processes* **1989**, *89* (2−3), 187−203.
(35) Ling, C.; Cottrell, C. E.; Marshall, A. G. *Chemom. Intell. Lab. Syst.* **1986**, *1* (1), 51−58.
(36) Kaur, P.; O'Connor, P. B. *J. Am. Soc. Mass Spectrom.* **2006**, *17* (3), 459−468.
(37) Longnecker, K.; Kujawinski, E. B. *Geochim. Cosmochim. Acta* **2011**, *75* (10), 2752−2761.
(38) Bahureksa, W.; Borch, T.; Young, R. B.; Weisbrod, C. R.; Blakney, G. T.; McKenna, A. M. *Anal. Chem.* **2022**, *94* (32), 11382−11389.
(39) Hawkes, J. A.; D'Andrilli, J.; Agar, J. N.; Barrow, M. P.; Berg, S. M.; Catalán, N.; Chen, H. M.; Chu, R. K.; Cole, R. B.; Dittmar, T.; et al. *Limnol. Oceanogr. Meth.* **2020**, *18* (6), 235−258.
(40) Qi, Y. L.; Fu, P. Q.; Li, S. L.; Ma, C.; Liu, C. Q.; Volmer, D. A. *Sci. Total Environ.* **2020**, *713*, No. 136573.
(41) Zhang, Q. R.; Lv, J. T.; He, A. E.; Cao, D.; He, X. S.; Zhao, L. X.; Wang, Y. W.; Jiang, G. B. *Water Res.* **2023**, *243*, No. 120359.
(42) Kostyukevich, Y.; Kononikhin, A.; Popov, I.; Nikolaev, E. *Anal. Chem.* **2013**, *85* (11), 5330−5334.
(43) Zherebker, A.; Rukhovich, G. D.; Sarycheva, A.; Lechtenfeld, O. J.; Nikolaev, E. N. *Environ. Sci. Technol.* **2022**, *56* (4), 2729−2737.

https://doi.org/10.1021/acs.analchem.3c04651
Anal. Chem. 2024, 96, 522−530